A Journal of the Gesellschaft Deutscher Chemiker

Angewandte International Edition GDCh Chemie

www.angewandte.org

Accepted Article

Title: Multienzyme-Mimic Nanogels Synthesized by Biocatalytic ATRP and Metal Coordination for Bioresponsive Fluorescence Imaging

Authors: Meiyuan Qi, Hui Pan, Hongdou Shen, Xianmeng Xia, Chu Wu, Xiaoke Han, Xingyue He, Wei Tong, Xia Wang, and Qigang Wang

To be cited as: *Angew. Chem. Int. Ed.* 10.1002/anie.202002331

Link to VoR: https://doi.org/10.1002/anie.202002331

WILEY-VCH

10.1002/anie.202002331

WILEY-VCH

Multienzyme-Mimic Nanogels Synthesized by Biocatalytic ATRP and Metal Coordination for Bioresponsive Fluorescence Imaging

Meiyuan Qi, Hui Pan, Hongdou Shen, Xianmeng Xia, Chu Wu, Xiaoke Han, Xingyue He, Wei Tong, Xia Wang* and Qigang Wang*

Abstract: The attempts towards enzyme mimics to design simple, stable and efficient non-protein systems for achieving the performance of natural enzymes, especially attractive to realize highly specific cancer diagnosis and treatment, have become an emerging field in recent years. The features of enzyme mimics highlight the pivotal importance of active site components and also the supported network environment for integrating and stabilizing them. Herein, the metal cross-linked polymeric nanogels (MPGs) system has been prepared based on the transition metal Fe (II) ion-coordinate biocompatible acryloyl-lysine polymer brush by the proposed enzyme-catalyzed atomic transfer radical polymerization (ATRPase) method. The monoatomic and highly dispersed Fe ions in MPGs can both serve as the efficient cross-linkers of gel network, and interestedly also the vital active centers of multienzyme mimic of superoxide dismutase (SOD) and peroxidase (POD) activity. The comparable catalytic activity with conventional Fe-based nanozymes and higher thermal stability than the molecular enzyme mimics and natural horseradish peroxidase (HRP) have been conducted. Studies on both cells and animals verify that the efficient reactive oxygen species (ROS)-responsive bio-fluorescence imaging can be successfully realized based on the tandem catalysis of mimetic activities of MPGs.

Conventional nanozymes, most of which are metal compounds nanoparticles such as Fe_3O_4, MnO_2, V_2O_5, etc., have certain bioactivities mainly due to the catalytic function of transition metal at the compact nanoscale surface.[1] In nature, the binding pocket structure of biological enzymes offering favorable spatial microenvironment near the active center is especially essential for the high catalytic efficiency.[2] The features of enzyme highlight the pivotal importance of active site components and also the supported network environment for integrating and stabilizing them. Encouraging efforts have been made on the rational design of carbon-based peroxidase mimics by adjusting components and environment of active site to pursue the high activity and selectivity.[3] Metal−organic frameworks (MOFs) with nanocavity similar to enzyme pockets, synthesized by polydentate ligands and metal nodes, possess the best enzyme-like activities and have been attracting more and more attention.[4] Unlike to MOFs and other inorganic materials, hydrogels as a class of hydrophilic gel with a three-dimensional network structure and good biocompatibility have been applied in many aspects of biomedical fields. And the biomimetic and natural enzymes encapsulated in hydrogel systems have become a hot topic in biological research, due to the protection from structural alterations and subsequent deactivation of the enzymes, ensuring higher loadings and better substrate mobility for efficient catalysis. Xu et al. have reported that the biomimetic enzyme in hydrogel can attain superactivity and exceptional stability in the organic solvent for catalyzing reactions. It's believed that the porous structure and nanofibers in hydrogels as an adjustable microenvironment around the active centers can further improve the activities of artificial enzymes.[5]

Hydrogels at nanoscale, namely the nanogels, with both nanosize dimensional stability and the hydrophilic networks as well as fluid-like transport properties can serve as an ideal candidate for further in vivo bio-applications.[6] Despite of the previous excellent work on the macrogel preparation technique, there is still a challenge to realize the modification or assembly in a confined nanospace to obtain the hybrid nanogels.[7] An acid-catalyzed proton reaction to trigger self-assembly of small molecules to obtain the supramolecular hydrogel fibers at the nanoscale surfaces has been proposed by van Esch group.[8] In authors' group, the cationic polysaccharides have been crosslinked by laccase-medicated polymerization at nanosurface.[9] While, in addition to the reported supramolecular self-assembly of peptide molecules or cross-linked polysaccharide derivatives on the nanosurface, there is not any reported work about the polymeric nanogels by the interfacial controlled radical polymerization and metal coordination.

In this work, an enzyme-catalyzed atomic transfer radical polymerization (ATRPase) method has been firstly proposed and the biocompatible polymer brushes can be obtained by the interfacial polymerization of amino acid (*N*-acryloyl-L-lysine) monomers. Then the metal coordinated polymeric nanogels (MPGs) have been finally constructed by the coordination effects between amino acid groups and transition metal Fe (II) ions and exhibits efficient multienzyme-like activities (superoxide dismutase (SOD) and peroxidase (POD)) simultaneously. Herein, Fe (II) ions in the MPGs are monoatomic and highly dispersed in the hydrophilic networks, which can both serve as the cross-linker of gel network and also the vital active center of the mimic enzymes, which exhibit the excellent reaction rate due to their spatial structure and high

[a] M. Qi, H. Pan, H. Shen, X. Xia, C. Wu, X. Han, X. He, Dr. X. Wang and Prof. Q. Wang
School of Chemical Science and Engineering
Tongji University
1239 Siping Road, Shanghai 200092, P. R. China
E-mail: 15174@tongji.edu.cn; wanggq66@tongji.edu.cn
[b] W. Tong
High Magnetic Field Laboratory, Chinese Academy of Sciences
350 Shushanhu Road, Hefei 230031, P. R. China

Supporting information for this article is given via a link at the end of the document.

enzyme mimics density in nanogel. Considering the relatively higher level of superoxide free radicals ($O_2^{-\cdot}$) in tumor environment,[10] the efficient reactive oxygen species (ROS)-responsive bio-fluorescence imaging has been successfully realized on the tumor-bearing mice, by using the tandem catalysis of multienzyme-mimic MPGs with activities of SOD and POD.

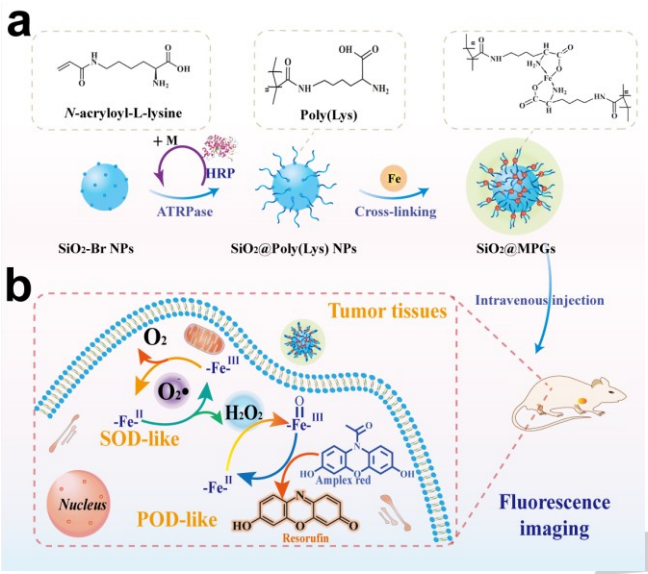

Scheme 1. Schematic illustration of MPGs synthesized by ATRPase for ROS responsive bio-fluorescence imaging in vivo. (a) Preparation process of SiO_2 cored MPGs (SiO_2@MPGs). (b) Mechanism illustration of ROS responsive fluorescence imaging by tandem catalysis of SiO_2@MPGs.

The multienzyme-mimic MPGs were synthesized by biocatalytic ATRPase route and applied for bio-fluorescence imaging as depicted in Scheme 1. Firstly, L-lysine was modified with acryloyl chloride to obtain the biocompatible monomer *N*-acryloyl-L-lysine as gelator (Figure S1, S2). And the core nanoparticles (SiO_2 NPs) were synthesized and modified with the halogen initiators successively to obtain SiO_2-Br NPs (Figure S3).[11] Poly-amino acid brushes on the surface of nanoparticles (SiO_2@Poly (Lys) NPs) were further synthesized by horseradish peroxidase (HRP)-assisted interfacial ATRP method, by using acryloyl L-lysine as the monomer and SiO_2-Br NPs as the initiator in the presence of reducing agent under oxygen-free conditions. What's interesting is that monomers containing carboxyl groups (-COOH) are not suitable for ordinary ATRP using transition metals as catalyst while it works in this enzyme-catalyzed ATRP process. The MPGs around the silica core nanoparticles (SiO_2@MPGs) were finally obtained by the coordination of Fe (II) ions and the L-lysine brush to form the stable di-amino acid coordination iron structure. Notably, the nanogels network can be cross-linked and further strengthened due to metal coordination, and the mono-dispersed and abundant Fe (II) ions can simultaneously act as the active center of catenulate lysine coordination iron mimic enzymes in the hydrogel network. By fully considering the structure-function relationships, the MPGs can facilitate the optimal interaction between the active center and substrate contact sites in the stable gel network, leading to the excellent enzyme-mimic catalytic efficiency for further ROS responsive fluorescence imaging by tandem reactions (Scheme 1b).

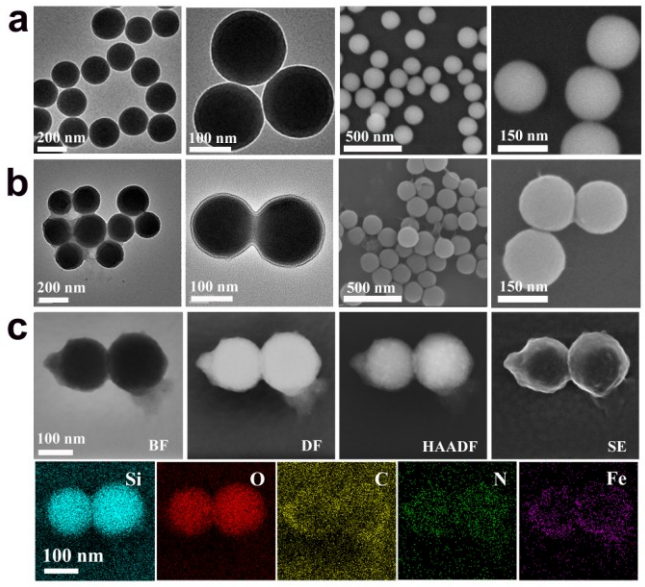

Figure 1. TEM and SEM images of (a) SiO_2 NPs and (b) SiO_2@MPGs; (c) STEM image and element mapping of Si, O, C, N, and Fe of SiO_2@MPGs.

The structures and physicochemical properties of SiO_2@MPGs were investigated as shown in Figure 1-3 and Figure S4-9. As shown in the typical transmission electron microscopy (TEM) images and scanning electron microscope (SEM) images in Figure 1a and 1b, SiO_2@MPGs have a more rough surface compared with the SiO_2 cores and show significant core-shell structure, with the MPG layer of about 10 nm. And the more obvious shell structure can be observed in scanning transmission electron microscopy (STEM) as shown in Figure 1c. The major elements including Si, C, N, O, and Fe can be detected by Energy Dispersive Spectrometer (EDS) (Figure S4). The homodispersed Fe elements (about 3.30 mg Fe elements per 1g SiO_2@MPGs) also verify the favorable coordination dispersion of the active center in MPGs. Both the increased average hydrodynamic sizes and the changes in zeta potential test during the preparation indicate the success of the modification process (Figure S5, S6). The characteristic peak at 1635 cm^{-1} (C=O stretching) and the decrease of the peaks at 1046 cm^{-1} (Si-O-Si stretching), 950 cm^{-1} (Si–OH bending) and 792 cm^{-1} (Si–O–Si bending) of silica structure in Fourier transform infrared spectroscopy (FT-IR) spectra (Figure S7) also verify the successfully grafting procedures.[12] The ingredient of hydrogel layer in SiO_2@MPGs was further analyzed by thermo gravimetric analysis (TGA), (Figure S8) with the 33.1% total weight loss of SiO_2@MPGs as 1g SiO_2 NPs containing 0.3764g hydrogels.

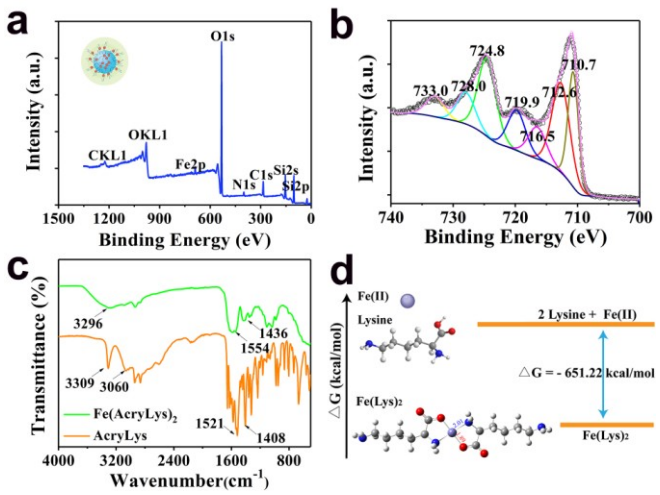

Figure 2. (a) XPS survey spectrum of SiO_2@MPGs. (b) Fe 2p XPS spectra and corresponding fitting curves obtained by using Avantage 5.976 software. (c) FT-IR spectra of *N*-acryloyl-L-lysine and AcryLys-Fe. (d) Gibbs Free energy diagram of the coordination reaction.

The typical characteristics of Fe (II) and Fe(III) in complexes of SiO_2@MPGs can be observed in the X-ray photoelectron spectroscopy (XPS) survey spectrum (Figure 2a,2b, and S9), the peaks appearing at about 710.7 eV and 724.8 eV were assigned to Fe (II), and 712.6 eV correspond to Fe(III), other peaks were attributed to the satellite peaks.[13] Meanwhile, the peaks of amino groups in *N*-acryloyl-L-lysine coordination iron (AcryLys-Fe) at 3309 cm^{-1}, and the carboxyl groups at 1521 cm^{-1} and 1408 cm^{-1} in *N*-acryloyl-L-lysine (AcryLys) were broadened and shifted respectively, indicating the strong coordination force between Fe and amino acid by FT-IR as shown in Figure 2c.[14] An obvious peak at around 294 nm in the ultraviolet-visible absorption spectrum (UV-vis) (Figure S10) further illustrates the coordination cross-linking of Fe (II) in nanogels, due to the transition of electronic energy levels in the molecules.[15] The density functional theory (DFT)-computed Gibbs free energy diagram of the most favorable pathway leading to the $Fe(Lys)_2$ and the molecular orbital energies indeed ensure the formation and the high chemical stability of the $Fe(Lys)_2$ (Figure 2d, S11).

The efficient multienzyme-like (SOD and POD) activities of SiO_2@MPGs were further investigated as shown in Figure 3, and schematic illustration of the catalytic reactions of SiO_2@MPGs with different substrates was shown in Figure S12. The electron paramagnetic resonance (EPR) test confirmed that the Fe(III) intermediate existed during the catalytic process (Figure S13). So based on the catalytic process of the traditional Fe(II)-centered SOD and the simulated calculation of POD-like catalytic process, the suggested mechanism of the SOD-like and POD-like activity of MPGs was illustrated in Figure 3a and 3b. MPGs has the similiar two electron-transfer catalytic mechanism with the high valent iron complex intermediates to the natural HRP of precise oxidative ability and in absence of $OH^{\bullet}$ during the catalytic process, other than the single electron-transfer mechanism of Fe-based nanozyme particles, which may offer the higher biocatalytic specificity and safety. Then, the SOD-like activity of SiO_2@MPGs was confirmed by WST method, as displayed in Figure 3c.[16] The change of absorbance in the SiO_2@MPGs group was inhibited obviously compared with the control group with the inhibition rate of about 46.9%, indicating the favorable SOD activity of SiO_2@MPGs. Subsequently, the POD-like activity of SiO_2@MPGs was demonstrated by typically TMB color reaction, and the absorbance band at 652 nm originated from the oxidation product of TMB is observed obviously in the presence of SiO_2@MPGs and H_2O_2, as shown in Figure 3d. In addition, Michaelis-Menten kinetics of SiO_2@MPGs, MPGs, the conventional Fe-based nanozymes (Fe_3O_4 nanoparticles with similar diameter of about 30 nm),[1a] molecular enzyme mimics (free Hemin and $Fe(Lys)_2$) were investigated (Figure 3e and Figure S14 and the kinetic parameters were shown in Table S1 and Figure 3f. At the same mass concentration, the kinetic parameters k_{cat} of MPGs is comparable to the value of Fe_3O_4 nanoparticles. Relative to the typical molecular enzyme mimics, MPGs exhibit higher activity due to the relieved molecular aggregation within spatial structure of nanogel scaffolds. Besides, polymeric nanogel network of MPGs can preserve much higher stability and robustness (Figure S15). MPG has the comparable catalytic activity compared with conventional Fe-based nanozymes and higher thermal stability than the molecular enzyme mimics.

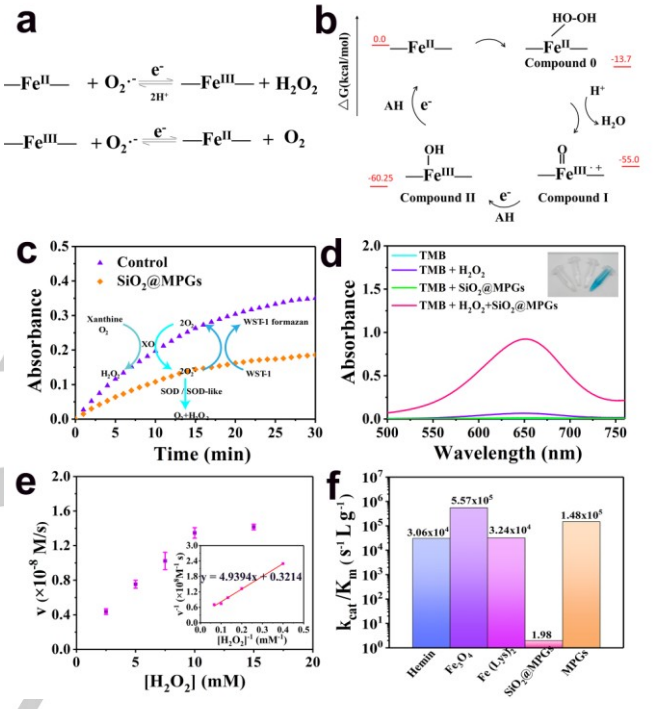

Figure 3. The suggested mechanism of (a) SOD-like and (b) POD-like activities of MPGs. (c) SOD-like activity measured by WST method. (d) The typical UV−vis absorbance spectra of POD-like activity. (e) Michaelis-Menten kinetics and double-reciprocal plots (the inset) of activities. (f) Comparison of catalytic efficiency of Hemin, Fe_3O_4, $Fe(Lys)_2$, SiO_2@MPGs and MPGs at the same mass concentration.

Furthermore, Amplex Red (AR) was chosen as the substrate to be oxidized to fluorescent substances (resorufin, $\lambda_{ex}/\lambda_{em}$ =570/590 nm) by MPGs as the POD (Figure S16a).[17] And within 15 minutes, the fluorescence intensity of resorufin increased gradually under different H_2O_2 concentrations (0-60 μM) (Figure S16b). The relationship between the fluorescence intensity and concentration of H_2O_2 presents positive correlation (Figure S16c), which can be further for efficient H_2O_2 responsive fluorescence imaging. Considering the high tandem catalysis activities of MPGs, the efficient ROS-responsive bio-fluorescence imaging can be achieved based on the superoxide free radicals ($O_2^{\bullet-}$) in tumor environment.[10] Before in vivo applications, the biocompatibility of SiO_2@MPGs was evaluated by the CCK-8 and fluorescence imaging method after incubation with 3T3 cells. As displayed in Figure 4a, SiO_2@MPGs show negligible cell cytotoxicity in all detected concentrations range. Also, the green fluorescence from living cells in the Calcein-AM staining test can also be found in the confocal fluorescence image, verifying the satisfying biocompatibility for further biological imaging use (Figure 4b). Schematic illustration of fluorescence imaging of SiO_2@MPGs enzyme mimics in vivo

has been shown in Figure 4c. The in vivo fluorescence imaging of tumor-bearing mice at pre, 0.5, 1, 3, and 6 h after intravenous injection of SiO_2@MPGs were conducted, as shown in Figure 4d. And the quantitative fluorescence intensity (photon counts) in the tumor region at different time were further recorded (Figure 4e). The apparent fluorescence signal of the tumor was detected as early as 1 h after the intravenous injection of SiO_2@MPGs. As we can see, the fluorescence signals in tumor tissue increased significantly along with the time, while that the signals of tumor tissues after intravenous injection of Amplex Red as the control were much lower (Figure S17). The subsequent fluorescence signals of the ex vivo tumor tissues also confirmed the high efficacy of SiO_2@MPGs as ROS responsive tumor imaging agent in the further. (Figure 4f, 4g). In addition, the main organs were stained with hematoxylin-eosin (H&E), and no tissue damage or inflammation was observed in heart, liver, spleen, lung, and kidney, which further confirmed the excellent safety of SiO_2@MPGs (Figure 4h and Figure S18).

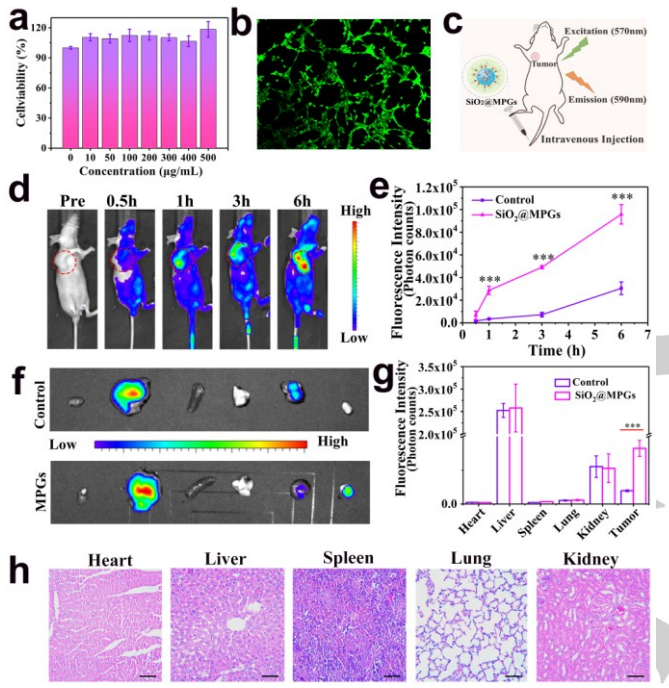

Figure 4. (a) Cytotoxicity of SiO_2@MPGs. The 3T3 cell viability after incubation with various concentrations of SiO_2@MPGs. (b) Confocal fluorescence imaging of 3T3 cells. (c) Schematic illustration of fluorescence imaging of SiO_2@MPGs in vivo. (d) Fluorescence imaging of tumor-bearing mice at different time after intravenous injection. (e) Fluorescence intensity (photon counts) in the tumor region at different times. n=3, ***P < 0.001. (f) Representative ex vivo fluorescence images of the tumors and main organs: Amplex red (top) and Amplex red/SiO_2@MPGs (bottom). (g) Fluorescence intensity (photon counts) in the ex vivo tumor region and main organs. n=3, ***P < 0.001. (h) H&E staining of heart, liver, spleen, lung, and kidney in the test group. Scale bar, 200 μm.

In summary, we developed an enzyme-catalyzed atomic transfer radical polymerization (ATRPase) method for interfacial controlled polymerization of biocompatible acryloyl L-lysine monomer chains, and high-efficient transition metal Fe (II) ions have been used as the cross-linkers to reinforce the hydrogel network to obtain the metal coordinated polymeric nanogel system (MPGs). The excellent multienzyme mimic activities of superoxide dismutase (SOD) and peroxidase (POD) can be realized due to the spatial structure and abundant enzyme mimics of highly dispersed square di-lysine coordination irons in the gel network. The absence of OH• during MPG catalytic process can lead to their more efficient and safer theranostic applications. The typical stability and activities of mimic enzyme have been investigated by XPS, FT-IR, UV-vis, EPR and DFT calculation and so on. MPGs around the silica core (SiO_2@MPGs) have achieved excellent enzyme-mimic catalytic efficiency for ROS responsive fluorescence imaging both in vitro and in vivo. The facile strategy of biocompatible monomer modification in the confined nanosurfaces by the ATRPase method and metal coordination cross-linking can be applied to further nanoplatform preparation for drug delivery and other biomedical applications. The further designs of nanogel-type enzyme mimics by screening amino acid ligands and metal active centers can form the diverse enzyme-like library with potential high catalytic activity and specificity.

Acknowledgements

This work was financially supported by the National Natural Science Foundation of China (No. 51773155, No. 51873156) and National Key Research and Development Program (No. 2016YFA0100800, No.2018YFC1803100). A portion of this work was performed on the Steady High Magnetic Field Facilities, High Magnetic Field Laboratory, CAS.

Conflict of interest

The authors declare no conflict of interest.

Keywords: ATRPase • bioresponsive • fluorescence imaging • mimic enzyme • nanogels

[1] a) L. Gao, J. Zhuang, L. Nie, J. Zhang, Y. Zhang, N. Gu, T. Wang, J. Feng, D. Yang, S. Perrett, X. Yan, *Nat. Nanotechnol.* **2007**, *2*, 577-583; b) Z. Wang, Y. Zhang, E. Ju, Z. Liu, F. Cao, Z. Chen, J. Ren, X. Qu, *Nat. Commu.* **2018**, *9*, 3334; c) F. Natalio, R. André, A. F. Hartog, B. Stoll, K. P. Jochum, R. Wever, W. Tremel, *Nat. Nanotechnol.* **2012**, *7*, 530-535; d) T. Sheng, J. Pan, Y. Xu, Q. Bao, P. Hu, J. Shi, *J. Inorg. Materi.* ***2019***, 34, 899-903.

[2] a) C. Chang, T. G. Traylor, *Proc. Natl. Acad. Sci. U. S. A.* **1973**, *70*, 2647-2650; b) J. Liao, *J. Med. Chem.* **2007**, *38*, 409-424; c) Z. Zhang, B. Zheng, Y. Wang, Y. Chen, G. Manco, Y. Feng, *Biochim. Biophys. Acta, Biomembr.* **2008**, *1784*, 1176-1183.

[3] a) M. S. Kim, J. Lee, H. S. Kim, A. Cho, K. H. Shim, T. N. Le, S. S. A. An, J. W. Han, M. I. Kim, J. Lee. *Adv. Funct. Mater.* **2020**, 30, 1905410. b) M. S. Kim, S. Cho, S. H. Joo, J. Lee, S. K. Kwak, M. I. Kim, J. Lee, *ACS Nano* **2019**, 13, 4312−4321; c) H. Sun, A. Zhao, N. Gao, K. Li, J. Ren, X. Qu, *Angew. Chem., Int. Ed.* **2015**, 54, 7176−7180.

[4] a) H. Cheng, Y. Liu, Y. Hu, Y. Ding, S. Lin, W. Cao, Q. Wang, J. Wu, F. Muhammad, X. Zhao, D. Zhao, Z. Li, H. Xing, H. Wei, *Anal. Chem.* **2017**, *89, 1552-11559*; b) Y. Wang, M. Zhao, J. Ping, B. Chen, X. Cao, Y. Huang, C. Tan, Q. Ma, S. Wu, Y. Yu, Q. Lu, J. Chen, W. Zhao, Y. Ying, H. Zhang, *Adv. Mater.* **2016**, *28*, 4149-4155.

[5] a) R. Jin, L. S. M. Teixeira, P. J. Dijkstra, C. A. Blitterswijk, M. Karperien, J. Feijen, *Biomaterials* **2010**, *31*, 3103-3113; b) S. Zhang, Q. Wei, Y. Shang, Q. Zhang, Q. Wang, *Chem. Commu.* **2017**, *53*, 12270-12273; c) Q. Wang, Z. Yang, X. Zhang, X. Xiao, C. K. Chang, B. Xu, *Angew. Chem. Int. Edit.* **2007**, *46*, 4285-4289; d) Z. Cui, S. Kim, J. J. Baljon, B. M. Wu, T. Aghaloo, M. Lee, *Nat. Commu.* **2019**, *10*, 3523; e) Q. Wang, Z. Yang, L. Wang, M. Ma, B. Xu, *Chem. Commu.* **2007**, *10*, 1032-1034.

[6] Q. Wu, Z. He, X. Wang, Q. Zhang, Q. Wei, S. Ma, C. Ma, J. Li, Q. Wang, *Nat. Commu.* **2019**, *10*, 240.

[7] a) Z. Yang, H. Gu, D. Fu, P. Gao, J. K. Lam, B. Xu, *Advanced Materials* **2004**, *16*, 1440-1444; b) R. Shenoy, M. W. Tibbitt, K. S. Anseth, C. N. Bowman, *Chem. Mater.* **2013**, *25*, 761-767.

[8] Y. Wang, F. Versluis, S. Oldenhof, V. Lakshminarayanan, K. Zhang, Y. Wang, J. Wang, R. Eelkema, X. Guo, J. H. Esch, *Adv. Mater.* **2018**, *30*, 1707408.

[9] a) X. Wang, D. Niu, P. Li, Q. Wu, X. Bo, B. Liu, S. Bao, T. Su, H. Xu, Q. Wang, *Acs Nano* **2015**, *9*, 5646-5656; b) X. Wang, D. Niu, Q. Wu, S. Bao, T. Su, X. Liu, S. Zhang, Q. Wang, *Biomaterials* **2015**, *53*, 349-357.

[10] a) P. E. Porporato, V. L. Payen, J. Pérez-Escuredo, C. J. Desaedeleer, P. Danhier, T. Copetti, S. Dhup, M. Tardy, T. Vazeille, C. Bouzin, O.

Feron, C. Michiels, B. Gallez, P. Sonveaux, *Cell Rep.* **2014**, *8*, 754-766. b) E. Panieri, M. M. Santoro, *Cell Death Dis*. **2016**, 7 , e2253. c) S. Vyas, E. Zaganjor, M. C. Haigis, *Cell*, **2016**, 3, 555-566.

[11] a) W. Stöber, A. Fink, E. Bohn, *J. Colloid. Interf. Sci.* **1968**, *26*, 62-69; b) X. Peng, Z. Wang, M.Zeng, Y. Liu, J. Zou, Z. Zhu, W. Deng, *J. Inorg. Materi.* **2019**, 34, 734-740.

[12] a) L. Qiao, X. Wang, Y. Gao, Q. Wei, W. Hu, L. Wu, P. Li, R. Zhu, Q. Wang, *Nanoscale* **2016**, 8, 17241–17249; b) L. Zhou, W. Yuan, J. Yuan, X. Hong, *Mater. Lett.* **2008**, *62*, 1372-1375.

[13] a) S. Manivannan, I. Kang, K. Kim, Langmuir **2016**, *32*, 1890-1898; b) G. Bhargava, I. Gouzman, C. M. Chun, T. A. Ramanarayanan, S. L. Bernasek, *Appl. Surf. Sci.*, **2007**, *253*, 4322-4329. c) Y. Chen, Z. Li, J. Hu, S. Peng, L. Rong, Y. Sun, X. Zhang,. Nanoscale Horiz. **2020**.(DOI: 10.1039/c9nh00583h)

[14] X. Zhang, Z. Yang, W. Li, L. Yang, S. Weng, J. Wu, *Spectrochim. Acta. A*. **2004**, *60*, 235-240.

[15] a) H. L. Friedman, *J. Am. Chem. Soc.* **1952**, *74*, 5-10; b) W. Gao, Y. Huang, R. He, X.-a. Zeng, *Int. J. Biol. Macromol.* **2018**, *108*, 1242-1247.

[16] K. Fan, J. Xi, L. Fan, P. Wang, C. Zhu, Y. Tang, X. Xu, M. Liang, B. Jiang, X. Yan, L. Gao, *Nat. Commu.* **2018**, *9*, 1440.

[17] a) V. G. Grivennikova, A. V. Kareyeva, A. D. Vinogradov, *Redox Biol.* **2018**, *17*, 192-199; b) V. Mishin, J. P. Gray, D. E. Heck, D. L. Laskin, J. D. Laskin, *Free Radical Biol. Med.* **2010**, *48*, 1485-1491.

10.1002/anie.202002331

WILEY-VCH

Entry for the Table of Contents

COMMUNICATION

Multienzyme-Mimic nanogels which were synthesized by a novel biocatalytic ATRPase and metal coordination technique exhibited efficient superoxide dismutase (SOD) and peroxidase (POD) activities for bioresponsive fluorescence imaging by tandem catalysis successfully.

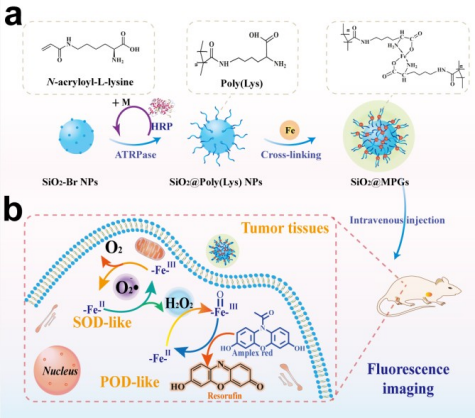

Meiyuan Qi, Hui Pan, Hongdou Shen, Xianmeng Xia, Chu Wu, Xiaoke Han, Xingyue He, Wei Tong, Xia Wang and Qigang Wang**

Page No. – Page No.

Multienzyme-Mimic Nanogels Synthesized by Biocatalytic ATRP and Metal Coordination for Bioresponsive Fluorescence Imaging